Organic & Biomolecular Chemistry

Accepted Manuscript

ROYAL SOCIETY OF CHEMISTRY

www.rsc.org/obc

Journal Name

ARTICLE

One probe, two-channel imaging of nuclear and cytosolic compartments with orange and red emissive dyes†

Received 00th January 20xx,
Accepted 00th January 20xx

DOI: 10.1039/x0xx00000x

www.rsc.org/

Demar R. G. Pitter,[a] Adrienne S. Brown,[a] James D. Baker[b] and James N. Wilson*[a]

Several new DNA-targeting probes that exhibit binding-induced 'turn on' fluorescence are presented. Two of the dyes, orange emissive **1**, (E)-4-(4(-4-methylpiperazin-1-yl)phenyl)6-(4-(4-methylpi-perazin-1-yl)styryl)pyrimidin-2-ol), and red emissive **2**, (E)-4-(4(-4-methyl-piperazin-1-yl)-phenyl)6-(4-(4-methylpiperazin-1-yl)styryl)-1,3-propanedionato-κO,κO']difluoroborane), are brightly fluorescent when bound to DNA, but are virtually non-fluorescent in aqueous solutions. Confocal fluorescence microscopy of live BT474, MCF7 and HEK293 cells demonstrates that both probes are cell permeable and rapidly accumulated intracellularly into cell nuclei and the cytosol. Taking advantage of their environmental sensitivity, these two pools of fluorophores are readily resolved into separate channels, and thus, a single dye allows two-color imaging of the nuclear and cytosolic compartments.

Introduction

Small molecule fluorescent probes are widely employed as imaging agents in microscopy and as readouts in biomolecular assays.[1-4] DNA-binding dyes are some of the most commonly utilized probes as they enable identification of individual cells via their nuclei and provide a frame of reference for other subcellular targets.[5-8] While several classes of dyes are available as nuclear stains, some limitations to their universal application persist. DAPI and the family Hoechst dyes require UV excitation (< 400 nm), which can damage cells. Cyanine dyes offer longer wavelength excitation and emission spectra, but their cationic structures make interactions with RNA, mitochondria or acidic vesicles unavoidable.[8-10]

In an effort to introduce new fluorescent stains that address these limitations, we recently reported two new DNA-binding dyes, Miami Green and Miami Yellow (**MG** and **MY**, Fig. 1), which incorporate a tunable donor-acceptor-donor scaffold and exhibit large emission enhancements, i.e. turn-on emission, upon binding to DNA.[11,12] Unlike cyanine dyes, such as the STYO® series, they can exist in a neutral form, allowing facile diffusion across membranes, yielding staining times and patterns similar to 4',6-diamidino-2-phenylindole (DAPI) or Hoechst 33242. Compared to the latter dyes, **MG** and **MY** are excited at longer wavelengths, 405 and 514 nm, respectively, eliminating the need for harmful UV excitation. We

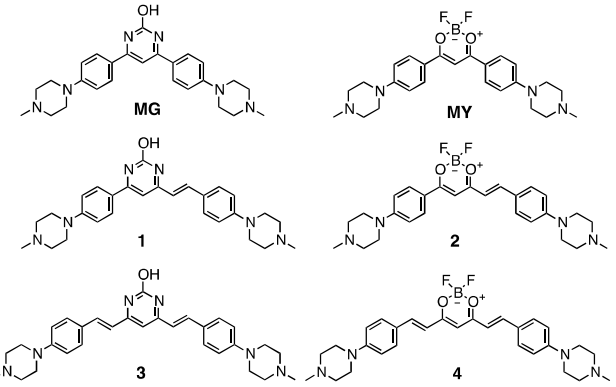

Fig. 1 Chemical structures of parent DNA-binding dyes, **MG** and **MY**, and newly synthesized compounds **1**-**4**.

hypothesized that expansion of the aromatic core of **MG** or **MY** could further shift their excitation (and emission) wavelengths providing additional imaging options compatible with yellow to red excitation sources while minimizing spectral overlap with common biomolecular tags such as blue, cyan or green fluorescent proteins.

In this contribution we explore four expanded analogues (**1**-**4**) of **MG** and **MY** produced via the introduction of one (**1**, **2**) or two (**3**, **4**) vinyl bridges between the electron-withdrawing core and the electron-donating aniline arms. Optical spectroscopy reveals that **1** and **2** retain the high turn-on ratios of the parent compounds and furthermore, they can differentiate between DNA and other cellular binding sites through shifts in their excitation and/or emission spectra. Doubly substituted compounds **3** and **4** were also evaluated, but were found to not exhibit high turn-on ratios and did not demonstrate the ability to differentiate between DNA, RNA and/or other cellular targets. Confocal microscopy demonstrated that **1** and **2** are rapidly

[a] *Department of Chemistry, University of Miami, 1301 Memorial Drive, Coral Gables, FL 33146, USA. E-mail: jnwilson@miami.edu; Fax: +1 305 284 4571; Tel: +1 305 284 2619*
[b] *Department of Biology, University of Miami, 1301 Memorial Drive, Coral Gables, FL 33146, USA*

†Electronic Supplementary Information (ESI) available: ^{1}H and ^{13}C NMR spectra, HOMO and LUMO density maps, additional optical spectra, coordinates of compounds for quantum chemical calculations. See DOI: 10.1039/x0xx00000x

accumulated in live cells and broadly distributed throughout the cytosol and nucleus. Interestingly, the cytosolic and nuclear populations of **2**, and to a lesser extent, **1**, can be separated into two imaging channels, allowing two-color resolution of these cellular compartments. This attractive behavior can be linked to the ability of the dyes to respond to subtle changes in their chemical microenvironment. While a 'turn-on' response can result through interaction with RNA or any number of protein binding folds present in the cytosolic milieu, probes bound to DNA exhibit redder excitation and emission spectra, which enables clear resolution of the nucleus. These dyes effectively combine the function of two separate dyes (i.e. a nuclear stain and a cytosolic stain) in a single probe. This behavior combined with their compatibility with standard laser lines (e.g. 458, 488, 514, 561 nm) or filter sets (e.g. GFP, FITC, YPF) suggests that these dyes should be useful probes for a number of imaging and screening applications.

Results and discussion

Design and Synthesis

We recently described parent compounds **MG** and **MY**; these dyes are optimally excited with 405 and 514 nm laser lines, respectively. Many additional excitation sources are typically available on both epifluorescent and confocal microscopes and we were motivated to develop probes that would match excitation wavelengths in the blue to cyan portion of the spectrum (≈ 450 to 500 nm) as well as redder excitation sources beyond the 514 nm used for **MY**. TD-DFT calculations at the 6-31G* level using the Gaussian quantum chemical suite[13] predicted that the optical transitions of these parent chromophores could be extended to redder wavelengths through the inclusion of one (**1**, **2**) or two vinyl groups (**3**, **4**) between the electron-donating arms and the electron-withdrawing core. The calculated spectra are shown in Fig. 2 suggest that the dyes should be compatible with excitation sources across the visible spectrum, including many common laser lines. The previously reported theoretical spectra for **MG** and **MY**, which are in good agreement with the experimentally observed spectra, are presented alongside the spectra for the newly synthesized compounds, **1**-**4**, as a reference.

The synthesis of **1** and **2** (Fig. 3) relied on the common diketo intermediate, **5**, which was synthesized via condensation of 1-[4-(4-methyl-1-piperazinyl)phenyl]-ethanone with ethyl acetate (Scheme 1). Cyclization of the diketo moiety with urea under acidic conditions produced **6**, with its electron-withdrawing hydroxypyrimidone core. Similarly, the electron-withdrawing core of **7** was prepared by reacting **5** with BF_3•Et_2O. Finally, condensation of **6** or **7** with 4-(4-methyl-1-piperazinyl)-benzaldehyde produced **1** and **2**, respectively. Symmetrical dyes **3** and **4** were prepared in one step by condensation of 4-(4-methyl-1-piperazinyl)-benzaldehyde with 4,6-dimethyl-2(1H)-pyrimidinone and difluoro-2,4-pentane-dionatoboron, respectively. The products were isolated in good to excellent yields as deeply colored solids that were readily soluble in polar organic solvents.

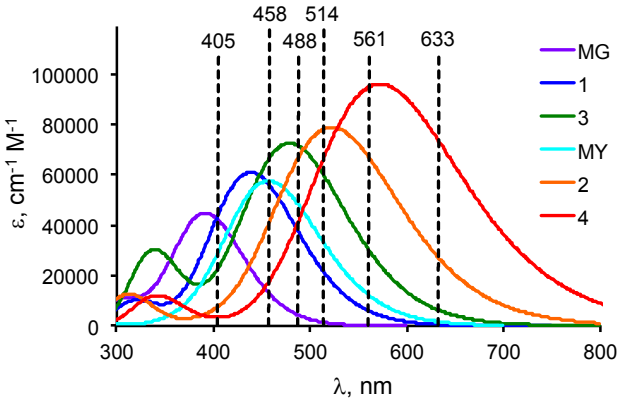

Fig. 2 Predicted absorption spectra of **1**-**4** compared with previously reported dyes, MG and MY; with increased conjugation length, excitation energies are significantly red-shifted and a pronounced hyperchromic effect is also predicted. Dashed lines are common excitation sources available for confocal microscopy. TD-DFT calculations[13] were performed at the 6-31G* level, using the B3LYP basis set and Truhlar's SMD solvent model (MeOH).[14]

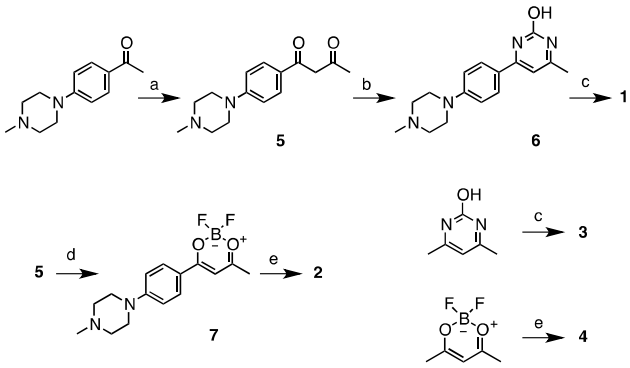

Scheme 1 Synthesis of **1**-**4**. Reagents and conditions: a) NaH, EtOH, EtOAc, 0° C, 24h; b) urea, 10% HCl in EtOH, 80° C, 12 h; c) 4-(4-methyl-1-piperazinyl)-benzaldehyde, TMS-Cl, DMF, 90° C, 48 h; d) BH_3, benzene, 25° C, 24 h; e) 4-(4-methyl-1-piperazinyl)-benzaldehyde, *t*Bu-NH_2, $B(OEt)_3$, toluene, 70° C, 48 h.

Optical Spectroscopy

The structures of **1**-**4**, with their donor-acceptor-donor motif, suggest that these dyes should be highly sensitive to the polarity of their microenvironment due to the formation of excited states with significant charge transfer (CT) character. Indeed, the fluorescence of solutions of **1**-**4** in less polar solvents can readily be detected by eye, while in more polar solvents, their emission is quenched (Fig S2). Binding to DNA may also induce enhancements in fluorescence, through reduction of the interactions with solvating water molecules as well as limiting twisting of the π system and reducing access to twisted intramolecular charge transfer (TICT) states. We therefore evaluated the optical properties of **1**-**4** in phosphate buffered saline (PBS) solutions, pH 7.2, in the absence and presence of calf thymus DNA (ctDNA).

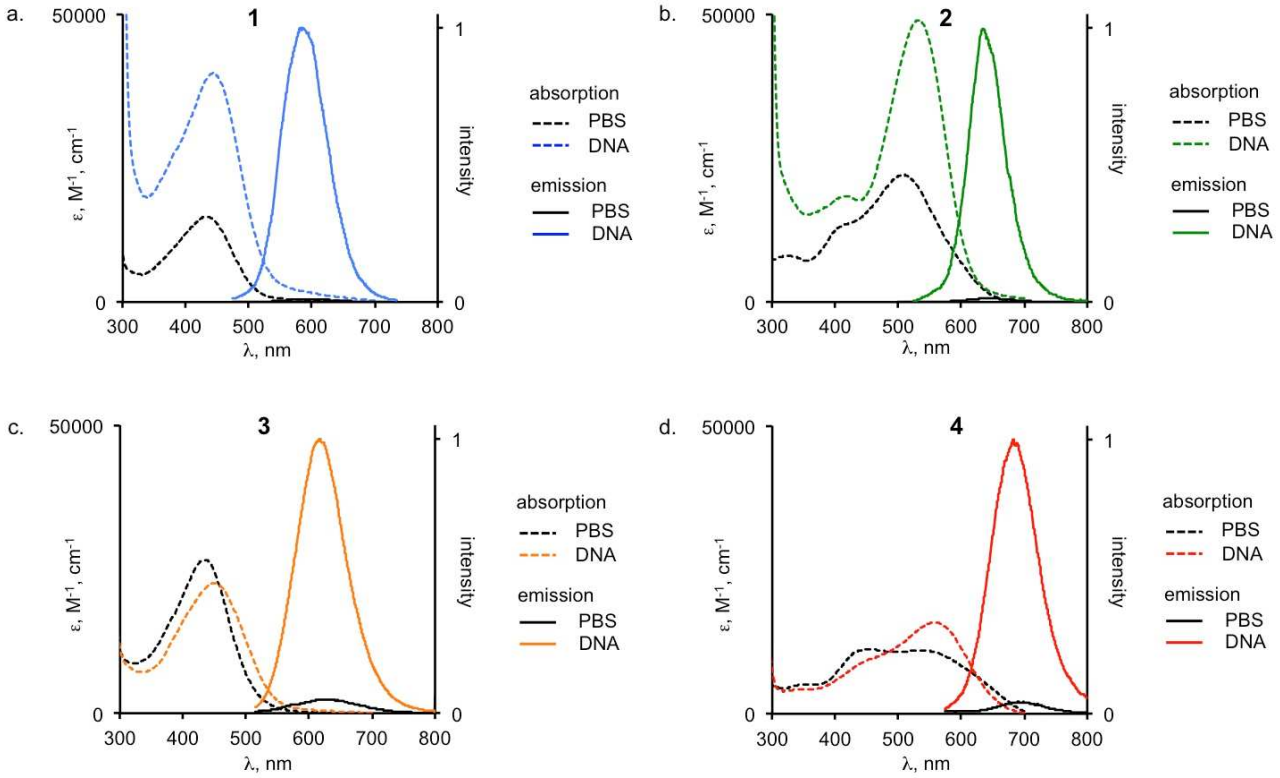

Fig. 3 Absorption and emission spectra of 1 μM solutions of **1**-**4** (a-d, respectively) in PBS in the presence (colored lines) and absence (black lines) of ctDNA (500 μM). For **1** and **2** a significant hyperchromic effect is observed upon binding while emission enhancements are observed for all compounds binding to DNA. Quantum yields are noted in Table 1.

The absorption and emission spectra of **1**-**4** are shown in Fig. 4 with key photophysical parameters summarized in Table 1; additional solvents are presented in the ESI (Table S1). The most striking feature is the emission enhancement observed for the probes in the presence of ctDNA. For **1** and **2**, emission is increased 92- and 64-fold, respectively, with quantum yields of photoemission (ϕ_{em}) of 0.44 for **1** and 0.13 for **2**. Moderate emission enhancements were observed for **3** and **4** when bound to DNA, with increases of approximately 10-fold for both dyes, while quantum yields remained relatively low, 0.02 for **3** and 0.003 for **4**. The poor optical performance of **3** and **4** is also observed in organic solvents (Table S1) and may be a result of their extended conjugation, which while achieving longer wavelength excitation and emission, could also lead to more polarized excited states and enhanced quenching.

Inspection of the absorption spectra also revealed marked changes for **1** and **2**, with more moderate changes for **3** and **4**. Pronounced hyperchromicity and a slight bathochromic shift were observed for the first pair of dyes. With molar absorptivities (ε) of 39,000 and 49,000 M^{-1} cm^{-1}, respectively, the overall brightness (ε • ϕ_{em}) of the dyes are 17,000 M^{-1} cm^{-1} for **1** and 6,300 M^{-1} cm^{-1} for **2**. These values compares favorably with many commercially available probes such as DAPI[15] and the Hoechst family[16] of dyes.[§] Though the molar absorptivities (Fig. 2) of **3** and **4** were predicted to be higher than **1** or **2**, the observed values are much lower, and in the case of **4**, the appearance of a prominent peak at higher excitation energies (≈ 450 nm) suggests the formation of H-type aggregates.[17] For both **3** and **4**, solubility appears to be a limiting factor and aggregation may contribute to a lower observed molar absorptivity. Indeed, at concentrations approaching 5 μM, PBS solutions of **3** and **4** became slightly turbid, confirming that the dyes were aggregating. In organic solvents, such as methanol, the molar absorptivities are much closer to their predicted values and solubility is not an issue.

Table 1. Summary of optical parameters of DNA-bound dyes.

cpd	$\lambda_{max, abs}$ (nm)	ε (M^{-1}, cm^{-1})	$\lambda_{max, em}$ (nm)	ϕ_{em}[a]
1	452	39,000	582	0.44
2	532	49,000	636	0.13
3	557	16,000	617	0.02
4	449	23,000	683	0.003

[a] ± 10%

Confocal Microscopy

We next examined the fluorescence properties of the two promising dyes, **1** and **2**, via confocal microscopy. Live, adherent BT474, MCF7 and HEK293 cells were exposed to 2 μM solutions of the probes by diluting 100x DMSO stock solutions directly into the cell culture media with rapid mixing; cell membranes were counterstained with CellMask Deep

Red™. The probes rapidly accumulated in the cells and within 15 minutes, intracellular fluorescence could be observed.‡ Given the spectral overlap with several laser lines, we explored different excitation wavelengths for the dyes, including 405, 458, 476 and 488 nm, for **1**, and 488, 496, 514 and 561 nm in the case **2**. Interestingly, using two different excitation wavelengths and selecting specific emission windows, we observed that emission from different cellular components could readily be resolved into two channels, as depicted in Fig. 4. In the case of **1**, the blue channel (Fig. 4a) revealed diffuse emission in the cytosol with nucleoli also visible; the green channel (Fig. 4b) showed emission localized to the nucleus, with the nucleoli strongly fluorescent. Overlaying these two channels, and a third red channel corresponding to a plasma membrane dye (Fig. 4c) reveals a clear contrast between the nuclear and cytosolic compartments, with emission from the nucleoli visible as cyan due to the overlap of the blue and green emission. For **2**, similar behavior was observed: the cytosol could be resolved into a blue channel (Fig. 4d), while the nuclei were captured in the green channel (Fig. 4e). In the case of **2**, staining of the nucleoli was not observed in either the blue or green channels, contrasting with the staining pattern of **1**. Additionally, the demarcation between the cytosol and nucleus is much clearer in the case of **2** as virtually no cyan fluorescence is visible to the eye in Fig 4f.

To gain some insight into the origin the two pools (blue and green channels) of fluorescent probes, we obtained the emission spectra from different regions of the cells, using the λ mode of the microscope, and compared them with possible cellular targets. Not surprisingly, the emission of both **1** and **2** from the nucleus corresponds very well with the emission spectra of the dyes in DNA solutions (Fig. 5c and 5d). Nucleoli are centers of ribosome synthesis and we hypothesized that **1** may be interacting with RNA at these sites, yielding a complex with a different optical signature than that observe for **1** + DNA. We therefore examined the optical spectra of **1** in the presence of RNA (Fig. 5a) for comparison with the spectra of **1** + DNA and the emission of **1** from the nucleoli. Both the emission and excitation spectra of **1** + RNA show small (≈ 10 nm), but non-trivial blue shifts compared to the spectra of **1** + DNA. The emission from the cytoplasm and from the nucleoli are also blue-shifted relative to the emission spectra observed for **1** + DNA or from the nucleus (excluding the nucleoli). The most important feature that distinguishes the RNA and DNA spectra, is the presence of a broad "red" shoulder in the excitation spectrum of **1** + DNA (Fig. 5c). At approximately 500 nm, this shoulder is half the height of the excitation maximum (450 nm); in the case of **1** + RNA, the height is only about 10% of the maximum value. The K_D values for **1** + DNA and **1** + RNA, obtained from saturating titrations (Figure S3), are very close at 2.5 and 2.9 μM, respectively. These results are consistent with the observed staining pattern with areas rich in both RNA and DNA overlapping in the blue and green channels.

Thus, **1** bound to DNA can be selectively excited with the 496 nm laser line and allowing clear resolution of the cell nuclei into the green channel shown in Figure 4b. Excitation at 458 nm can result in emission from **1** interacting with either

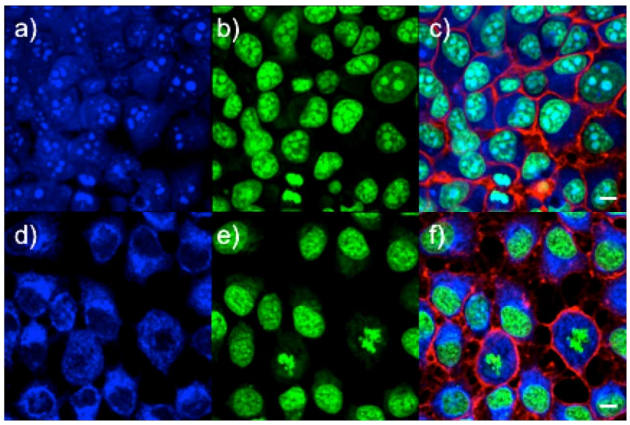

Fig. 4 Confocal fluorescence microscopy of live BT474 cells treated with **1** (top row) and MCF7 cells treated with **2** (bottow row). Emission the cytosol is resolved into the blue channel (**a**,**d**), while the nuclei are visualized in green (**b**,**e**). The overlays of the two channels, plus a red channel for the membrane stain are at the right (**c**,**f**). Excitation wavelengths and emission windows are shown below in Fig 5. Scale bars are 10 μm.

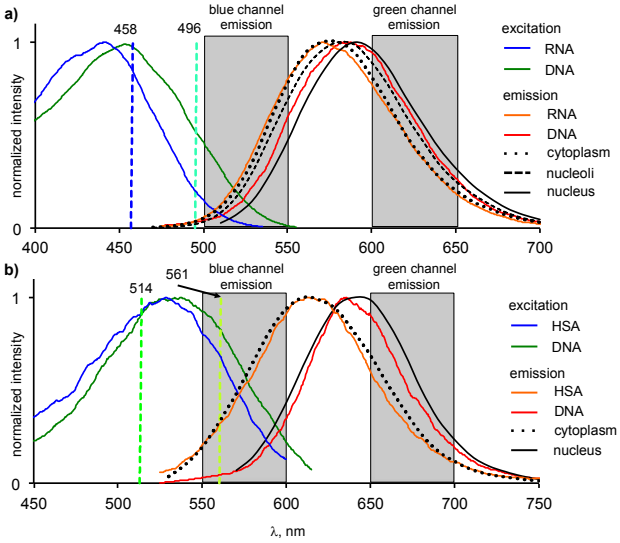

Fig. 5 Comparison of excitation and emission spectra overlaid with imaging parameters for blue and green channels in Fig. 4. **a)** Excitation and emission spectra of **1** in complex with RNA or DNA compared to emission from the cytoplasm, nucleoli and nucleus. **b)** Excitation and emission spectra of **2** in complex with HSA or DNA compared to emission from the cytoplasm and nucleus.

RNA or DNA as well as complexes of **1** with any other possible binding folds present in the complex cellular milieu.

The lack of nucleoli staining with **2** suggested that RNA was not a major intracellular target of this dye. Indeed, while the K_D value for **2** + DNA was found to be 0.6 μM (Figure S3), the K_D for **2** + RNA could not accurately be measured due to inner filter effects at high concentrations and is greater than ~10 μM. Therefore, we examined the possibility that **2** may interact with hydrophobic pockets of a protein to produce the blue channel shown in Fig. 4d and the cytoplasmic emission spectrum shown in Fig. 5b. Human serum albumin (HSA) is a

globular carrier protein with multiple binding sites[18] and is a suitable test protein for examining the binding of **2** to hydrophobic pockets. The emission of **2** in the presence of HSA is blue-shifted by 20 nm relative to the spectrum of **2** + DNA and matches very well with the emission obtained from the cytosol of cells treated with **2**. While the excitation spectra of **2** + DNA and **2** + HSA overlap significantly and excitation at 514 nm results in emission from both populations, the emission spectrum of **2** + HSA has a strong blue edge that is not present in the spectrum of **2** + DNA. This emission is captured in the blue channel and is limited to the cytosol. Conversely, excitation at 561 nm favors the DNA-bound population, which combined with the green channel capturing emission between 650-700 nm, leads to emission being almost exclusively from the nucleus.[§§]

Conclusions

We have generated orange and red emissive DNA-binding dyes, **1** and **2**, that exhibit high turn-on ratios and attractive staining patterns in live cells. Compared to commercially available nucleus stains, these new compounds offer a few advantages. First, they fill a spectroscopic gap between some of the most commonly employed nucleic acid dyes, such as the blue-emissive DAPI or Hoechst 33342 and red-emissive DRAQ5.[8] Second, in addition to staining cell nuclei, they can also serve as cytosolic stains, with each compartment easily resolved into a unique color captured in separate imaging channels. While some commercially available compounds do stain both the nucleus and cytoplasm, they do not provide clear delineation of the two compartments, whereas **1** and **2** do. Acridine orange is one well-known dye that does exhibit two-color staining, however, in our hands uptake of acridine orange required much longer exposure times (2 h) compared to **1** and **2**. Finally, these dyes demonstrate a more general property of fluorophores that can be employed to simultaneously image multiple targets in unique channels. Spectroscopic characterization of specific and "nonspecific" staining may reveal small, but non-trivial shifts in excitation or emission wavelengths that allows resolution of distinct populations of fluorescent probes.

The authors declare no competing financial interests.

Experimental

General Methods

Reagents and solvents were obtained from commercial suppliers and used without further purification. ^{1}H NMR and ^{13}C NMR spectra were recorded on a 500 MHz spectrometer. Unless otherwise noted, absorbance spectra were obtained as previously described[19] using probe concentrations of 10 μM; fluorescence studies were performed using probe concentrations of 1 μM. For determination of ϕ_{em}, solutions were prepared to an optical density of 0.05 or less in order to minimize inner filter effects. Perylene in cyclohexane was used as a reference for quantum yields.[20]

Computational Methods

Quantum chemical calculations were carried out utilizing the Gaussian '09 suite of electronic structure modeling software.[12] Ground state geometries of the dyes were optimized by DFT with the B3LYP/6-31G(d) method using Truhlar's SMD solvation model.[14] Vertical transition energies were obtained by TD-DFT calculations with the B3LYP/6-31G(d) with the SMD model. Molecular orbitals were visualized using the GaussView 5 program. The coordinates of optimized geometries are provided in the Supporting Information.

Synthesis

***Synthesis of 1-(4-(4-methylpiperazyn-1-yl)phenyl)-butane-1-3-dione* (5):** To a nitrogen-purged 25 mL Schlenk flask charged with a stirbar and containing 0.25 g of sodium hydride, 10 mL of anhydrous ethanol was added by syringe at 0 ºC. To this mixture, 2.0 g of anhydrous ethyl acetate (20.5 mmol) was added while stirring. After 5 min, 3.0 g (13.7 mmol) of 4-(4-methyl-1-piperazinyl)-ethanone dissolved in anhydrous THF were added by syringe. After stirring for 24 h at room temperature, the mixture was quenched with the addition of 5% HCl solution, extracted three times with ethyl acetate, dried over anhydrous MgSO4. Crystallization from isopropanol produced 2.50 g (70%) of **5** as a beige powder; mp. 324-326 °C (decomp.); IR ν_{max} (cm-1): 3357.7, 2975.4, 2941.1, 1568.1, 1380.5, 1289.1, 1201.4, 785.8; 1H NMR (500 MHz, DMSO-d6 TFA) (major tautomer): δ 2.19 (s, 3H), 2.81 (s, 3H), 3.26 (broad s, 8H), 6.46 (s, 1H), 7.07-7.08 (d, 2H, J = 5.0 Hz), 7.88-7.86 (d, 2H, J = 10.0 Hz); ^{13}C NMR (125 MHz, DMSO-d6, TFA): δ 25.07, 31.08, 44.63, 52.43, 95.93, 114.64, 124.68, 129.37, 130.97, 158.57, 184.42, 191.20; HR-ESI (Q-TOF) m/z: calc'd for $C_{15}H_{21}N_2O_2^+$ $[M+H]^+$: 261.3445, found 261.1609.

***Synthesis of 1-(4-(4-methylpiperazin-1-yl)phenyl)-1,3-propane-dionato-κO, κO']difluoro-borane* (6):** 1.0 g (3.8 mmol) of 1-(4-(4-methylpiperazyn-1-yl)phenyl)butane-1-3-dione was placed in a nitrogen-purged 25 mL Schlenk flask charged with a stirbar. The flask was then capped and 10 mL of anhydrous benzene followed by 5 ml (40.5 mmol) of boron trifluoride diethyl etherate were added by syringe. The reaction was then stirred at room temperature for 24 h. Excess boron trifluoride diethyl etherate was evacuated and benzene solvent evaporated, the resultant orange slurry was then triturated with ethyl acetate to produce **6** as an orange precipitate that was collected by vacuum filtration. (0.862 g, 72%); mp 242-244 °C (decomp.); IR ν_{max} (cm^{-1}): 3672.9, 2978.9, 1559.9, 1055.4, 976.3; ^{1}H NMR (500 MHz, DMSO-d_6): δ 2.21 (s, 3H), 2.29 (s, 3H), 2.41-2.42 (t, 4H J = 5.0 Hz), 3.51-3.53 (t, 4H, J = 10.0 Hz), 6.95 (s, 1H), 7.06-7.08 (d, 2H, J = 10.0 Hz), 7.99-8.01 (d, 2H, J = 10.0 Hz); ^{13}C NMR (125 MHz, DMSO-d_6): δ 24.25, 42.51, 43.89, 52.35, 96.63, 114.27, 119.22, 132.25, 154.94, 180.21, 188.97; HR-ESI (Q-TOF) *m/z*: calc'd for $C_{15}H_{20}BF_2N_2O_2^+$ $[M+H]^+$: 309.1433, found: 309.1601.

***Synthesis of 4-methyl-6-(4-(4-methylpiperazin-1-yl)phenyl)-pyrimidin-2-ol* (7):** 1.0 g (3.8 mmol) of 5, 1.38 g (23 mmol) of urea, 2.0 mL of HCl and 10.0 mL of isopropanol were mixed in a 20 mL pressure tube with a magnetic stirbar. After monitoring the reaction by TLC, the reation was cooled to room temperature and quenched with concentrated sodium hydroxide; the resultant yellow precipitate was then filtered and dried under vacuum. (0.37 g, 34%); mp 325-330 °C; IR ν_{max} (cm^{-1}): 3680.3, 2983.9, 2899.8, 1643.1, 1619.1, 1584.3, 1240.9, 1203.0, 1065.9, 814.0; ^{1}H NMR (500 MHz, DMSO-d_6): 2.22 (s, 6H), 2.42-2.44 (t, 4H, J = 10.0 Hz), 3.29-3.31 (t, 4H, J = 10.0 Hz), 6.791 (s, 1H), 7.00-7.02 (d, 2H, J = 10.0 Hz), 7.95-7.97 (d, 2H, J = 10.0 Hz); ^{13}C NMR (125 MHz, DMSO-d_6, TFA): δ 19.65, 42.44, 44.52, 52.29, 100.02, 114.92, 123.84, 130.08, 152.77, 155.48, 161.25, 167.43; HR-ESI (Q-TOF) *m/z*: calc'd for $C_{16}H_{20}N_4O^+$ $[M+H]^+$: 285.3705, found: 285.1734.

***Synthesis of (E)-4-(4(-4-methylpiperazin-1-yl)phenyl)6-(4-(4-methylpiperazin-1-yl)styryl)pyrimidin-2-ol* (1):** 0.30 g (1.0 mmol) of 4-methyl-6-(4-(4-methylpiperazin-1-yl)phenyl)pyrimidin-2-ol, 0.27 g (1.3 mmol) of 4-(4-methyl-1-piperazinyl)-benzaldehyde, 2.40 g (19.0 mmol) of TMS-Cl, and 10 ml of anhydrous dimethylformamide were mixed in a 25 mL pressure tube with a magnetic stirbar. After heating at 90 ºC for 2 days, the reaction was cooled to room temperature and quenched with concentrated sodium hydroxide; the precipitate was isolated by filtration. **1** was crystallized from isopropanol, resultant orange flakes were filtered and dried under vacuum. (0.20 g, 40%); mp 400 °C (decomp.); IR ν_{max} (cm^{-1}): 3672.1, 2978.1, 2903.2, 1604.4, 1549.2, 1448.5, 1236.6, 1076.0, 1066.2, 1054.7, 820.5, 791.7; ^{1}H NMR (500 MHz, DMSO-d_6, TFA): δ 2.87 (s, 3H), 3.15, (broad s, 4H), 3.23-3.25 (d, 4H, J = 10.0 Hz), 3.56 (broad s, 4H), 4.12-4.14 (d, 2H, J = 10.0 Hz), 4.26-4.29 (d, 2H, J = 15.0 Hz), 6.94-6.97 (d, 1 H, J = 15.0 Hz), 7.15-7.16 (d, 2H, J = 10.0 Hz), 7.20-7.22 (d, 2H, J = 10.0 Hz), 7.61-7.63 (d, 2H, J = 10.0 Hz), 8.11-8.13 (d, 2H, J = 10.0 Hz), 8.30-8.33 (d, 1H, J = 15.0 Hz), 10.12-10.19 (d, 2H, J = 35.0 Hz); ^{13}C NMR (125 MHz, DMSO-d_6, TFA): δ 42.19, 44.05, 44.51, 52.64, 52.74, 97.03, 113.13, 114.68, 115.05, 118.80, 125.70, 130.37, 131.21, 147.47, 148.84, 152.38, 153.79, 161.45, 161.48; HR-ESI (Q-TOF) *m/z*: calc'd for $C_{28}H_{34}N_6O^+$ $[M+H]^+$: 471.6285, found: 471.2897.

***Synthesis of (E)-4-(4(-4-methylpiperazin-1-yl)-phenyl)6-(4-(4-methylpiperazin-1-yl)styryl)-1,3-propanedionato-κO, κO']difluoroborane* (2):** 1.00 g (3.2 mmol) of 2, 0.73 g (3.55 mmol) of 4-(4-methyl-1-piperazinyl)-benzaldehyde, 0.82 g (3.6 mmol) of tributyl borate, 0.03 g (0.35 mmol) of tert-butylamine and 10 mL of toluene were mixed in a 25 mL round bottom flask with a stirbar and heated to 70 ºC. After 48 h, the reaction was cooled and concentrated under reduced pressure. The resulting residue was purified over alumina (1:1 Ethyl acetate to methanol eluent), followed by triturated with methanol to produce a red powder as a precipitate that was collected by vacuum filtration. (73.0 mg, 5%); mp 327-330 °C; IR ν_{max} (cm^{-1}): 3133.2, 1600.5, 1521.5, 1557.7, 1397.8, 1036.2, 973.3, 925.6; ^{1}H NMR (500 MHz, DMSO-d_6): δ 2.22 (s, 3H), 2.43 (broad s, 8H), 3.5 (broad s, 8H), 6.85-6.88 (d, 1H, J = 15.0 Hz), 7.01-7.03 (d, 2H, J = 10.0 Hz), 7.08-7.10 (d, 2H, J = 10.0 Hz), 7.64-7.65 (d, 2H, J = 5.0 Hz), 7.83-7.86 (d, 2H, J = 15.0 Hz), 7.96-7.98 (d, 2H, J = 10.0 Hz); ^{13}C NMR (125 MHz, DMSO-d_6): δ 46.01, 46.08, 46.51, 46.95, 54.65, 54.71, 96.14, 113.69, 114.62, 117.06, 119.35, 124.14, 131.48, 131.57, 145.38, 153.41, 155.42, 177.56, 177.90; HR-ESI (Q-TOF) *m/z*: calc'd for $C_{27}H_{33}BF_2N_4O_2^+$ $[M+H]^+$: 494.3938, found: 495.4013.

***Synthesis of 4,6-bis(4-(4-methylpiperazin-1-yl)styryl)pyrimidin-2-ol* (3):** 0.37 mg (3.0 mmol) of 4,6-dimethylpyrimidone, 1.50 g (7.3 mmol) of 4-(4-methyl-1-piperazinyl)-benzaldehyde, 2.40 g (19.0 mmol) of TMS-Cl, and 10 ml of anhydrous dimethylformamide were mixed in a 25 mL pressure tube with a magnetic stirbar. After heating at 90 ºC for 2 days, the reaction was cooled to room temperature and quenched with concentrated sodium hydroxide; the precipitate was isolated by filtration. **3** was crystallized from isopropanol, resultant yellow flakes were filtered and dried under vacuum. (0.41 g, 82%); mp 400 °C (decomp.); IR ν_{max} (cm^{-1}): 3678.1, 2974.9, 1741.2, 1630.7, 1601.4, 1543.9, 1294.3, 1142.0, 1007.5, 973.4, 825.0; ^{1}H NMR (500 MHz, DMSO-d_6, TFA): δ 1.99 (s, 6H), 3.13-3.16 (broad d, 4H J = 15.0 Hz), 3.19-3.22 (broad d, 4H, J =15.0 Hz) 3.51-3.53 (d, 4H, J = 10.0 Hz), 4.10-4.13 (d, 4H, J = 15.0 Hz), 6.92-6.95 (d, 2H, J = 15.0 Hz), 7.14-7.15 (d, 4H, J = 5.0 Hz) 7.524 (s, 1H), 7.60-7.62 (d, 4H, J = 10.0 Hz), 8.19-8.22 (d, 4H, J = 15.0 Hz), 10.570 (broad s, 1H); ^{1}H NMR (500 MHz, MeOD, TMS-Cl): δ 2.37 (s, 6H), 2.63-2.64 (d, 8H, J = 5.0 Hz), 6.80-6.83 (d, 2 H, J = 15.0 Hz), 6.953 (s, 1H), 7.00-7.02 (d, 4H, J = 10.0 Hz), 7.57-7.59 (d, 4H, J = 10.0 Hz), 7.76-7.79 (d, 2H, J = 15.0 Hz); ^{13}C NMR (125 MHz, MeOD-d_6,): δ 23.15, 45.00, 54.51, 101.43, 115.46, 124.15, 127.80, 128.21, 134.59, 151.31, 165.30, 169.78, 179.12. HR-ESI (Q-TOF) *m/z*: calc'd for $C_{30}H_{36}N_6O^+$ $[M+H]^+$: 497.6654, found: 497.3043.

***Synthesis of 4,6-bis(4-(4-methylpiperazin-1-yl)-styryl)-1,3-propane-dionato-κO, κO']-difluoroborane* (4):** 3.10 g (15.1 mmol) of 4-(4-methyl-1-piperazinyl)-benzaldehyde, 1.10 g (7.5 mmol) difluro-2,4-pentanedianatoboron, 1.73 g (7.5 mmol of tributyl borate, 0.110 g (1.5 mmol) of tert-butylamine and 15 ml of toluene were mixed in a 25 mL round bottom flask with a stirbar and heated at 70 °C. After 48 h the reaction was cooled and the precipitate filtered and rinsed with toluene. The precipitate was then recrystallized in isopropanol. (160 mg, 40%); mp 325-329 °C; IR ν_{max} (cm^{-1}): 3579.2, 2741.4, 1595.3, 1543.4, 1492.5, 1392.7, 1057.9, 995.7, 974.5, 822.4; ^{1}H NMR (500 MHz, DMSO-d_6,): δ 2.858 (s, 6H), 3.12-3.16 (t, 8H, J =20.0 Hz) 3.52-3.53 (d, 8H, J = 10.0 Hz), 4.12-4.15 (t, 8H, J = 15.0 Hz), 6.386 (s, 1H), 6.97-7.00 (d, 2H, J = 15.0 Hz) 7.09-7.11 (d, 4H, J = 10.0 Hz), 7.77-7.79 (d, 4H, J = 10.0 Hz), 7.89-7.92 (d, 2H, J = 15.0 Hz): ^{13}C NMR (125 MHz, DMSO-d_6, TFA): δ 40.86, 42.52, 44.53, 52.39, 101.83, 115.28, 117.61, 125.30, 132.09, 146.54, 152.31, 178.56 HR-ESI (Q-TOF) *m/z*: calc'd for C29H36$BF_2N_4O_2^+$ $[M+H]^+$: 521.4393, found: 521.2905.

Confocal Microscopy

BT474, MCF7 and HEK293 cells were cultured as previously described in sterile T-75 flasks.[19,21] Cells were maintained in RPMI or DMEM containing 10% dialyzed FBS, penicillin (100 units/mL) and streptomycin (0.01%) solution under a humidified 5% CO_2 atmosphere. For imaging, cells were seeded at a density of 10^5 cell/cm^2 in 96 microwell plates. Cells maintained a normal morphology during the course of the experiments (maximum of 2 h) and remained adhered to the imaging plate. Confocal fluorescence microscopy was performed on a Leica SP5 housed within the UM Biology Imaging Core Facility.

Acknowledgements

This work was supported by the National Cancer Institute Innovative Molecular Analysis Technologies Program, CA182341-01 (J.N.W.). J.N.W. also acknowledges the support of the Bankhead-Coley New Investigator Research Program, 3BN08. The National Science Foundation is acknowledged for providing funds towards the purchase of an LC-ESI-MS (CHE-0946858).

Notes and references

‡ HEK293 cells stained with **2** exhibited large vesicles or granules containing the probe, regardless of staining concentration.

§ As noted in references 15 and 16, the quantum yield of photoemission for DAPI and Hoechst 33258 vary greatly depending on the concentration and identity of the target DNA. For direct comparison with **1** and **2**, we obtained ϕ_{em} of the dyes (1 μM) with 500 μM ctDNA and calculated the brightness values ($\varepsilon \bullet \phi_{em}$) accordingly. For DAPI, $\phi_{em} = 0.44$ and $\varepsilon \bullet \phi_{em} = 11{,}100$ M^{-1} cm^{-1}; for Hoechst 33258, $\phi_{em} = 0.88$ and $\varepsilon \bullet \phi_{em} = 24{,}800$ M^{-1} cm^{-1}.

§§ Excitation spectra cannot be obtained from the imaged samples due to the lack of a broad spectrum excitation source. Thus, the excitation spectra obtained in solution may not correspond to the actual excitation spectra of the probes in cells or tissue; additional small shifts in peak position or cutoffs may lead to further selectivity using the parameters shown above.

1 M. S. Gonçalves, *Chem. Rev.,* 2009, **109,** 190.
2 R. W. Sinkeldam, N. J. Greco and Y. Tor, *Chem. Rev.,* 2010, **110**, 2579.
3 B. N. B. Giepmans, S. R. Adams, M. H. Ellisman and R. Y. Tsien, *Science,* 2006, **312**, 217.
4 B. A. Armitage, *Curr. Opin. Chem. Biol.,* 2011, **15**, 806.
5 L. S. Ploeger, H. F. Dullens, A. Huisman and P. J. van Diest, *Biotech. Histochem.,* 2008, **83**, 63.
6 K. Glaser, K. Wilke, R. Wepf and S. S. Biel, *Skin Res. Technol.,* 2009, **14**, 324.
7 T. Suzuki, K. Fujikura, T. Higashiyama and K. Takata, *J. Histochem. Cytochem.,* 1997, **45**, 49.
8 P. J. Smith, M. Wiltshire, S. Davies, L. H. Patterson and T. Hoy, *J. Immunol. Methods*, 1999, **229**, 131.
9 J. Kapuscinski, *J. Histochem. Cytochem.,* 1990, **38**, 1323.
10 Vlodkowic, D.; Skommer, J.; Darzynkiewicz, Z. SYTO Probes in the Cytometry of Tumor Cell Death. *Cytometry A*, 2008, ***73A***, 496.
11 D. R. G. Pitter, J. Wigenius, A. S. Brown, J. D. Baker, F. Westerlund and J. N. Wilson, *Org. Lett.*, 2013, **15**, 1330.
12 J. N. Wilson, J. Wigenius, J.; D. R. G. Pitter, Y. Qiu, M. Abrahamsson and F. Westerlund, *J. Phys. Chem. B*, 2013, **117**, 12000.
13 M. J. Frisch, G. W. Trucks, H. B. Schlegel, G. E. Scuseria, M. A. Robb, J. R. Cheeseman, G. Scalmani, V. Barone, B. Mennucci, G. A. Petersson, H. Nakatsuji, M. Caricato, X. Li, H. P. Hratchian, A. F. Izmaylov, J. Bloino, G. Zheng, J. L. Sonnenberg, M. Hada, M. Ehara, K. Toyota, R. Fukuda, J. Hasegawa, M. Ishida, T. Nakajima, Y. Honda, O. Kitao, H. Nakai, T. Vreven, J. A. Montgomery Jr., J. E. Peralta, F. Ogliaro, M. Bearpark, J. J. Heyd, E. Brothers, K. N. Kudin, V. N. Staroverov, R. Kobayashi, J. Normand, K. Raghavachari, A. Rendell, J. C. Burant, S. S. Iyengar, J. Tomasi, M. Cossi, N. Rega, J. M. Millam, M. Klene, J. E. Knox, J. B. Cross, V. Bakken, C. Adamo, J. Jaramillo, R. Gomperts, R. E. Stratmann, O. Yazyev, A. J. Austin, R. Cammi, C. Pomelli, J. W. Ochterski, R. L. Martin, K. Morokuma, V. G. Zakrzewski, G. A. Voth, P. Salvador, J. J. Dannenberg, S. Dapprich, A. D. Daniels, Ö. Farkas, J. B. Foresman, J. V. Ortiz, J. Cioslowski and D. J. Fox, *Gaussian 09, Revision A.1*, Gaussian, Inc., Wallingford, CT, 2009.
14 A. V. Marenich, C. J. Cramer and D. G. Truhlar, *J. Phys. Chem. B*, 2009, **113**, 6378-6396.
15 P. Cavatorta, L. Masotti and A.G. Szabo, *Biophys. Chem.*, 1985, **22**, 11.
16 D. E. Comings, *Chromasoma*, 1975, **52**, 229.
17 A. Eisfeld and J. S. Briggs, *Chem. Phys.,* 2006, **324**, 376.
18 M. Fasano, S. Curry, E. Terreno, M. Galliano, G. Fanali, P. Narciso, S. Notari and P. Ascenzi, *Life*, 2005, **57**, 787.
19 J. N. Wilson, A. S. Brown, W. M. Babinchak, C. D. Ridge and J. D. Walls, *Org. Biomol. Chem.,* 2012, **10**, 8710.
20 I. Berlman, Handbook of Fluorescence Spectra of Aromatic Molecules, Academic Press, New York, 2nd edn, 1971.
21 E. Park, R. Baron and R. Landgraf, *Biochem*., 2008, **47**, 11992.